Arthur A. Salamatin

Detection of Microscale Mass-Transport Regimes in Supercritical Fluid Extraction

The problem of detecting supercritical fluid extraction regimes on the particle-scale level is discussed by using a generalized multiparameter model, which includes the shrinking-core (SC) and broken-and-intact-cells (BIC) approaches as its limiting cases. The model accounts for two internal mass-transfer resistances attributed to cell membranes and transport channels. A wide spectrum of particle-scale extraction regimes, described by the model, agree with available up-to-date relatively short laboratory experiments. Simplified concepts (like SC or BIC) could only be used for available experimental data correlation, and do not allow a reliable extension to long process times. The experimental methodology was suggested to detect limiting internal mass-transfer mechanisms.

Keywords: Broken-and-intact-cells model, Cell membrane permeability, Extraction curves, Mass transfer, Shrinking core model

Received: October 30, 2016; *revised:* January 05, 2017; *accepted:* January 16, 2017

DOI: 10.1002/ceat.201600599

1 Introduction

It is generally agreed that industrial development should proceed within the concept of so-called green chemistry [1]. In extraction technologies, this prompts the use of solvents under supercritical conditions, characterized by temperature and pressure higher than the solvent critical parameters. Supercritical solvents generally possess relatively high diffusivity and permeability, low viscosity, high (liquid-like) density, and tunable dissolution capacity, which are essentially affected by temperature and pressure [2]. Carbon dioxide (CO_2) is one of the most well-known and widely used green solvents.

Supercritical fluid extraction (SFE) technology [3–5] is a widely studied application of CO_2. It is traditionally used for the extraction of natural compounds from raw plant material (crushed seeds, ground petals, leaves, etc.). Before extraction, the polydisperse particles of ground material are loaded into a cylindrical vessel. The packed bed is filled by the solvent (CO_2) at the desired supercritical pressure (≈ 30 MPa) and temperature (≈ 308 K). The solvent saturates the raw material and dissolves target compounds. The extraction starts when the thermodynamic equilibrium is reached, and the solvent is pumped through the porous packed bed of plant material at a known flow rate. The dissolved extractable substances diffuse from the inside of the particles into the pore phase of the packed bed. The solvent transports the solute to the vessel outlet, and, finally, the solute is separated from the solvent by depressurization.

Practical implementation of the described technology requires essential economical investments [4, 6]. That is why SFE is studied intensively on the laboratory scale to understand the principal mechanisms of SFE phenomena, formulate mathematical models that allow simulation and optimization [5, 7–9] of the whole extraction process, and, eventually, minimize the costs. Conventionally, a sophisticated SFE description must distinguish between different mechanisms of the solvent mass transfer on the macroscale level of the porous packed bed in the vessel and on the microscale level of single particles. When the limiting mass-transfer mechanism on the microscale is detected, the methods of extraction-rate intensification can be developed.

Macroscale modeling is traditionally based on a spatially averaged hydrodynamic model of two-component solution flow through the porous packed bed of ground plant-material particles, generally accounting for axial dispersion effects [4–9]. One of the key challenges in SFE theory is to develop an adequate internal (microscale) submodel for the solute mass transfer in particles, which could be validated and constrained experimentally.

Different approaches to mass-transfer modeling in particles have been suggested recently [10–18]. This is a direct consequence of the plant-cell structure complexity, and insufficient knowledge of diffusive transport mechanisms in various cell compartments containing extractable target compounds. As a result, series of investigations [19–21] have been conducted to validate the developed microscale models by fitting the simulations to laboratory data.

Despite a remarkable diversity of internal submodels, only two limiting approaches are conventionally discussed and

Arthur A. Salamatin
arthur.salamatin2@gmail.com
Kazan Federal University, Department of Aerohydromechanics, Kremlyovskaya Str. 18, Kazan, 420008, Russia.

employed in SFE data interpretation; they are the original shrinking core (SC) model [11], extended later to the bidisperse packed-bed model [12], and the broken-and-intact-cells (BIC) model [13, 14]. The latter assumes high longitudinal permeability of the internal microscopic channels (cell walls), which results in a lumped parameter system approximation with the average solute concentration in the ground material. In contrast, the SC concept considers the case of high transversal permeability of the cell membranes and assigns all the mass-transfer resistance to diffusion along the transport channels. Consequently, the narrow diffusive front moves inside each particle and separates the shrinking oil-filled core from the outer depleted transport zone. Clearly, there is a wide intermediate range of the ground-plant-material properties when typical rates of solute diffusion across the cell membranes are on the same order as those through the particle, along its transport channels, and the two above limits (SC and BIC) fail to describe the whole spectra of SFE regimes on the microscale level.

Generally, the so-called overall extraction curve (OEC) is used for model constraining and identification. The curve is an integral macroscale characteristic and shows the total fraction of oil extracted from the substrate for any fixed moment of time. Starting from the beginning of the process, it changes gradually from zero to unity. Two main SFE stages are traditionally discerned in multiscale OEC: the initial, constant extraction rate (CER), linear stage, when the outlet pore-phase solute concentration is equal to the limiting saturation concentration, and the final stage of slow, nonlinear growth of the accumulated mass of solute, when the outlet concentration is extremely small. The very rapid transition between the two stages is characterized by a drastic decrease in the outlet solute concentration from its maximum to almost zero value. The duration of the first stage is determined mostly by the initial volume fraction of the so-called free oil. Within the framework of the BIC model, the free-oil receptacles are broken cells, whereas for the SC model they are the dust particles [12]. The residual oil stored in intact cells (for BIC approach) or the main fraction of ordinary particles (for the SC model) is mostly extracted during the nonlinear stage and is called tied oil. Importantly, the equivalent volume fraction of broken cells in the BIC approach to supply the same duration of the linear stage is slightly higher than the volume fraction of dust particles in the bidisperse SC model since superficial cells of ordinary particles also contribute to the initial stage duration [12]. The uncertainty in the determination of the free-oil volume fraction also contributes to the problem of particle-scale extraction regime detection.

As a rule, the duration of the linear extraction period as well as the OEC slope of the final nonlinear stage are used for model identification. Other SFE characteristics, such as outlet solute concentration in the pore phase and residual oil distribution in the ground plant material along the vessel, are very rare in observations [22, 23].

Despite essential conceptual differences, both simplified (SC- and BIC-) microscale submodels, described above, generally provide a similar degree of agreement with the available OEC data. Therefore, detection of the solute transport regime on the particle-scale level becomes a nontrivial theoretical and experimental problem using macroscale data only. The main goal of this study is to analyze feasible microscale transport mechanisms involved in the SFE process and understand how they manifest themselves on the macroscale level to explore the ways to discern different SFE regimes and appropriately specify the internal submodel.

With this in mind, a generalized microscale SFE model for mass transfer in particles that reproduces principal structural features of the raw material was formulated. It includes solute dissolution inside cells, as well as solute diffusion across cell membranes and along transport channels. The proposed approach covers all mass-transport mechanisms separately considered by the BIC and SC models, which are shown, with the use of scale analysis and numerical simulations, to be its particular limiting cases. It is demonstrated that a diversity of distinct extraction regimes can be observed on the particle scale in addition to the limiting ones. Further analysis shows that distinct features of various regimes are screened on the macroscale, and the normalized flux from the particle is the same during the tied-oil extraction at the relatively short times typical for laboratory experiments. When a larger amount of tied oil is extracted the normalized extraction rate decreases, and internal extraction regimes manifest themselves at high process time in different ways. The experimental methodology is suggested to detect adaptive parameters of general particle-scale submodels.

2 Mathematical Model

2.1 Submodel of Particle-Scale Transport

An adequate, sophisticated description of solute transport through the ground plant material and its exchange with the solvent in the pore phase is crucial for diagnostic simulations and underlies macroscale submodel formulation. Microscale modeling should also consider particle shape (flat or spherical) and size polydispersity, as well as solute solubility in the solvent. The mass-transfer mechanisms are strongly affected by the buildup of ground plant material, and diffusional resistance characteristics of various cell compartments.

In the suggested approach, each particle is assumed to be sphere of radius a[1)] and is considered to be an agglomerate of cells (Fig. 1) that form two continuous and interacting systems. They are the symplast, which is represented by internal parts of biological cells, in which the solute is initially stored as an undissolved oil (4) [24–27], and the apoplast composed of cell walls (2) and intercellular space (3). The apoplast plays the role of the solute-transport channels. The two systems are separated from each other by a permeable cell membrane (5) that surrounds every cell. The cells are considered as lumped systems containing solvent (1) with dissolved solute and inclusions (4) of undissolved extractable substances. Clearly, if the undissolved oil fraction exists in the cell then the concentration of the dissolved solute is close to the limiting solute saturation concentration θ_*. The cells also contain insoluble substances (6).

1) List of symbols at the end of the paper.

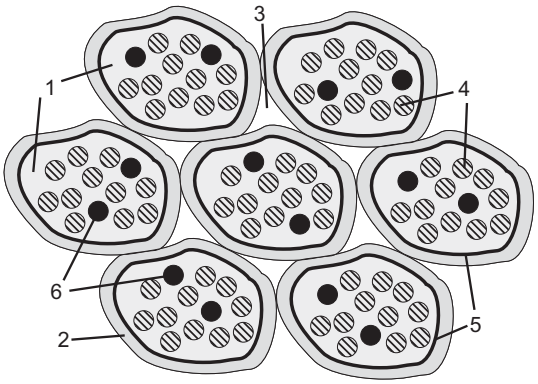

Figure 1. Schematic of the internal structure of ground particles: (1) solute, dissolved in the solvent; (2) cell wall; (3) intercellular space (voids); (4) undissolved oil; (5) cell membrane (solid line); (6) insoluble substances (proteins, etc.).

The described cell structure of the raw material is related to the intact cells of ordinary particles; the proposed particle-scale model is essentially focused on the tied-solute extraction. The free-oil receptacles formed after milling procedures should be considered individually.

The solute diffusion through the apoplast is traditionally assumed to be governed by Fick's law with apparent diffusion coefficient D_a, and the gradient of solute concentration θ_a is the driving force along channels. The average density x_s of the target compounds currently contained in cells is defined as the total mass of oil (including the one dissolved in the solvent and the undissolved oil) in a unit intracellular volume. The dissolved solute concentration in cells is designated as θ_s.

The basis of the proposed particle-scale submodel is the solute-dissolution process inside cells. As explained above, in general, oil is distributed within cells simultaneously among two phases during extraction. This situation takes place when the initial oil content exceeds the solvent dissolution capacity characterized by saturation concentration θ_*. During extraction, undissolved oil stored in oil inclusions is continuously consumed by the solvent, penetrating cells, and being instantaneously saturated up to the limiting concentration $\theta_s = \theta_*$, until the phase of the oil inclusions completely disappears, and θ_s becomes proportional to x_s, as shown in Eq. (1):

$$\theta_s = \min\{\theta_*; x_s/(1-\varepsilon_{is})\} \tag{1}$$

in which ε_{is} is the intracellular volume fraction, occupied by insoluble substances.

Only two diffusional resistances were distinguished in this study; one was assigned to the transport channels, and the other to the cell membrane, characterized by the reduced mass-transfer coefficient β_c, normalized by the mean cell radius. Thus, the proposed model incorporates the principal assumptions of both simplified BIC and SC approaches, and considers only one diffusional resistance (attributed to either the cell membrane or transport channels). The solute sorption/desorption effects [28] are not considered here.

The solute mass balance for a single cell is formulated as shown in Eq. (2):

$$(1-\varepsilon_a)\frac{\partial x_s}{\partial t} = -3(1-\varepsilon_a)\beta_c(\theta_s - \theta_a) \tag{2}$$

whereas for the apoplast the following equation is valid:

$$\varepsilon_a\frac{\partial \theta_a}{\partial t} = 3(1-\varepsilon_a)\beta_c(\theta_s - \theta_a) + D_a\Delta\theta_a \tag{3}$$

In these equations, t is time and ε_a is the apoplast volume fraction inside the particle. Δ is the Laplace differential operator in the radial direction due to the assumed spherical symmetry of the mass-transfer process.

According to Eq. (2), the concentration difference $\theta_s - \theta_a$ in two systems (symplast and apoplast) is the driving force of diffusion across the cell membrane. Eq. (3) states that the solute concentration in the apoplast varies due to its diffusive mass transfer out of the cell and further along transport channels according to Fick's law.

The initial and boundary conditions should be formulated for the searched characteristics x_s and θ_a in the reference particle

$$x_s|_{t=0} = x_s^0 \tag{4}$$

$$\left.\frac{\partial \theta_a}{\partial r}\right|_{r=0} = 0, \quad \theta_a|_{r=a} = c \tag{5}$$

in which $0 \le r \le a$ is the radial coordinate with the origin in the particle center, x_s^0 is the initial oil content in the plant material, and c is the pore-phase solute concentration at the particle surface. It is determined by the macroscale submodel, which describes solute filtration through the porous packed bed, and is discussed in detail in the literature [9, 11–14]. The initial condition in Eq. (4) is valid when either the preliminary stage of thermodynamic equilibrium establishment is disregarded and $c = 0$ at the beginning of the process, $t = 0$, or when $x_s^0 >> \theta_*$, and the amount of solute diffused from cells into the packed-bed pore phase as well as apoplast is negligible if compared with the total amount of oil [29].

2.2 Scale Analysis of the Internal Submodel

Generally, two typical times characterize the oil depletion from the spherical particle of radius a. They are the time of solute transfer across the cell membrane

$$T_{BIC} = \frac{x_s^0}{\theta_*}\frac{1}{3\beta_c} \tag{6}$$

and the time of dissolved-solute diffusion along transport channels

$$T_{SC} = \frac{x_s^0}{\theta_*}\frac{a^2}{6D_a} \tag{7}$$

Each of the respective timescales, defined by Eqs. (6) and (7), is a direct consequence of the BIC [13] and SC [12, 30] models,

and the corresponding BIC or SC regime occurs on the particle scale when $T_{BIC} >> T_{SC}$ or $T_{BIC} << T_{SC}$.

When both values are on the same order, $T_{SC} \approx T_{BIC}$, at comparable diffusional resistances, the intermediate extraction regime occurs on the particle scale. As a result, in the general case, the typical time of solute diffusion from the cell of the raw material to the particle surface can be envisaged as the sum of the two counterparts given by Eqs. (6) and (7):

$$T = T_{BIC} + T_{SC} = \frac{x_s^0}{\theta_*}\left(\frac{1}{3\beta_c} + \frac{a^2}{6D_a}\right) \tag{8}$$

The spatial scale is the particle radius a, whereas the concentrations x_s and θ_s, θ_a are accordingly normalized by x_s^0 and θ_*, respectively.

Eventually, mass-balance master Eqs. (1)–(3) governing solute diffusion inside a particle can be presented in terms of dimensionless time $\tau = t/T$, oil content inside cells $X_s = x_s/x_s^0$, and concentrations $\vartheta_s = \theta_s/\theta_*$, $\vartheta_a = \theta_a/\theta_*$ in the symplast and apoplast, respectively.

$$\delta_a \frac{M}{1+M}\frac{\partial \vartheta_a}{\partial \tau} = (1-\varepsilon_a)M(\vartheta_s - \vartheta_a) + \frac{1}{6}\Delta\vartheta_a \tag{9}$$

$$\frac{M}{1+M}\left((1-\varepsilon_a)\frac{\partial X_s}{\partial \tau} + \delta_a \frac{\partial \vartheta_a}{\partial \tau}\right) = \frac{1}{6}\Delta\vartheta_a \tag{10}$$

$$\vartheta_s = \min\left\{1; \frac{X_s}{\Theta}\right\} \tag{11}$$

Eqs. (9)–(11) contain four similarity criteria, i.e., the volume fraction ε_a of apoplast transport channels and

$$\delta_a = \varepsilon_a \frac{\theta_*}{x_s^0}, \quad M = \frac{T_{SC}}{T_{BIC}} = \frac{a^2\beta_c}{2D_a}, \quad \Theta = (1-\varepsilon_{is})\frac{\theta_*}{x_s^0} \tag{12}$$

The ε_a factor is a small parameter on the order of 0.01. Hence, ε_a and the apoplast oil accumulation terms, proportional to δ_a, can be neglected. So, diffusive mass transfer in the apoplast is considered in the quasi-stationary approximation.

By using this information, together with Eq. (11), the following reduced mass-balance equations

$$\frac{6M}{1+M}\frac{\partial X_s}{\partial \tau} = \Delta\vartheta_a, \quad 6M(\vartheta_s - \vartheta_a) + \Delta\vartheta_a = 0 \tag{13}$$

completed by the dimensionless analogs of the initial and boundary conditions from Eqs. (4) and (5)

$$X_s|_{t=0} = 1, \quad \left.\frac{\partial \vartheta_a}{\partial \xi}\right|_{\xi=0} = 0, \quad \vartheta_a|_{\xi=1} = c/\theta_* \tag{14}$$

form the generalized nonlinear model for oil extraction from ground plant particles. Here, $0 \le \xi = r/a \le 1$ is the normalized radial coordinate in the reference particle. Only two similarity numbers, Θ and M, specify the SFE regime on the particle-scale level since the normalized boundary solute concentration, c/θ_*, is typically small for tied-oil extraction. The sensitivity of microscale as well as macroscale extraction regimes to these dimensionless criteria is studied in Sects. 3.1 and 3.2 in which the key results of numerical simulations [31] are presented. Their physical meaning can be summarized as follows.

The Θ number quantitatively characterizes the initial amount of target compound in the raw material. The case of small $\Theta << 1$ generally corresponds to vegetable and fatty-oil extraction from oilseed (rapeseed, sunflower seed, pumpkin, apricot kernels, etc.), whereas $\Theta \approx 1$ assumes essential-oil extraction. The latter case is not considered here since mostly vegetable and fatty oil extraction possess the multiscale OECs, and the initial condition in Eq. (4) is not appropriate for the raw material at high Θ.

The M criterion, which is the ratio between the membrane and the intercellular diffusion rates, is the principal parameter that controls the internal extraction regime. Two limiting scenarios of small (I) and high (II) M values should be distinguished. Asymptotic expansion of Eq. (13) in case I, at $M \to 0$, leads to the BIC model as the principal-order approximation (to be published elsewhere). In case II, at $M \to \infty$ (and $\Theta << 1$), the SC model is derived. This theoretical statement is demonstrated below in computational experiments.

3 Results and Discussion

3.1 Internal Extraction Regimes: Sensitivity Tests

The M number is the principal parameter that controls the internal extraction regime. This is evidently revealed by oil-content profiles with respect to the dimensionless radial coordinate ξ inside a reference particle. The variability of X_s in different internal extraction regimes, for $10^{-2} < M < 10^3$, and their sensitivity to Θ are illustrated by Fig. 2 at $c = 0$. It is clear that the microscale extraction pattern closely follows the BIC approximation at $M < 10^{-1}$ with practically uniform X_s distribution and oil concentration in the apoplast, which is close to the pore-phase solute concentration, i.e., zero in this case. With an increase in M, a jump develops in the X_s profile, and an SC-type extraction regime sets on at $M > 10^2$. A moving transition zone, where the oil content in symplast drops from unity to Θ, becomes thinner as M tends to infinity, and its width, predicted by the scale analysis, is on the order of $O(M^{-0.5})$.

Different extraction regimes can occur on the particle-scale level, depending on diffusional characteristics (M criterion) of the cell membrane and transport channels. Some unique advanced technologies, such as magnetic resonance imaging (MRI) [29], may be potentially capable of distinguishing between various patterns of oil distribution on the particle scale. Conventional experimental techniques normally follow OEC during a certain period of time. Hence, only integral solute consumption from the particle is measured, and could be used for detecting the extraction regime.

3.2 Total Oil Extracted from the Particle

The total volume fraction $0 \le S(\tau) \le 1$ of oil extracted from the reference particle by the current moment τ was suggested in

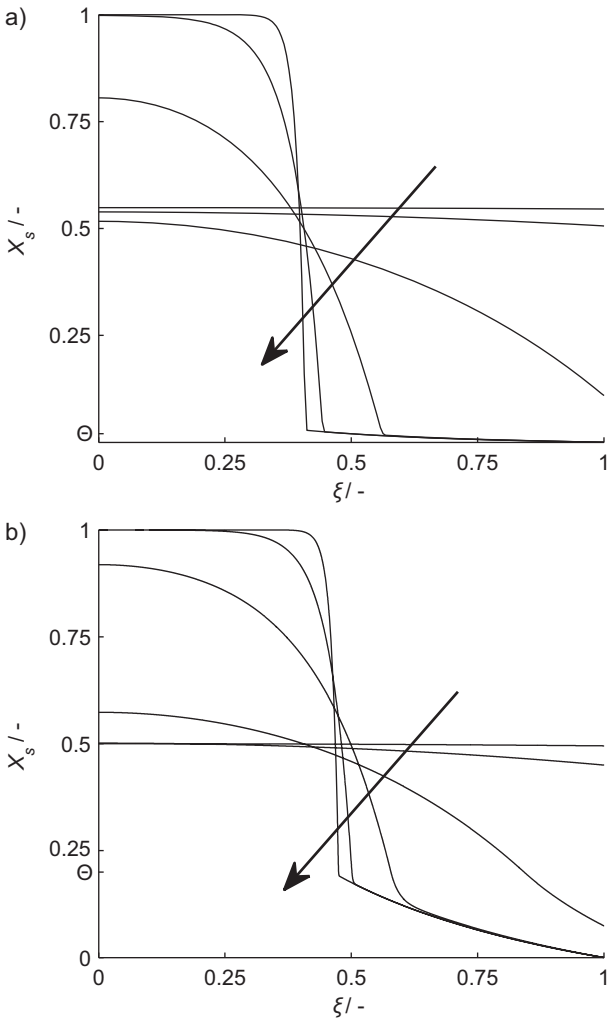

Figure 2. Distribution of the oil content in the particle at the same moments of normalized particle-extraction time, τ = 0.5, different *M* values, and (a) Θ = 0.02, (b) Θ = 0.2. Arrows indicate lg*M* increases in steps of 1 from –2 to 3.

the literature [12, 30] as a cumulative characteristic of the particle state.

$$S(\tau) = 1 - 3\int_0^1 \xi^2 X_s(\tau,\xi)\mathrm{d}\xi \tag{15}$$

The *S* function, or cumulative function, is closely related to OEC, which is traditionally used for model identification.

To clarify this point, a packed bed composed of ordinary (containing tied oil) spherical particles of volume fraction 1 - α with mean radius *a* is considered. If the volume fraction of free oil in the substrate is α and the corresponding cumulative function is $0 \le s \le 1$ then

$$Y(\tau) = \alpha\int_0^1 s(\tau,\zeta)\mathrm{d}\zeta + (1-\alpha)\int_0^1 S(\tau,\zeta)\mathrm{d}\zeta \tag{16}$$

in which $0 \le \zeta \le 1$ is the normalized axial coordinate in the vessel. After the free oil is depleted (s = 1) and the linear CER stage is finished at $\tau > \tau_{CER}$, the pore-phase concentration of the solute in the vessel tends to a minimum, $c/\theta_* \approx 0$, and, as predicted by simulations, *S* becomes practically uniform in the vessel with respect to ζ

$$Y(\tau) \approx \alpha + (1-\alpha)S(\tau), \quad \tau > \tau_{CER} \tag{17}$$

So, the correspondence between the measured OEC *Y* and cumulative curve *S* of a reference particle is established for various internal regimes. The extraction regime of a substrate is determined by the *M* parameter in the macroscopic model under consideration: monodisperse approximation of the ensemble of ordinary particles of volume fraction 1 – α and explicitly accounted free oil by means of cumulative function *s*. The variability of OEC, i.e., *Y*, with *M* is the same as the dependence of *S* on *M* examined below.

Note that the extraction rate in the ensemble of ordinary particles, i.e., $S(\tau)$ in Eq. (17), at $\tau > \tau_{CER}$ is only determined by the fraction $S_{CER} = S(\tau_{CER})$ of oil extracted during the initial stage. It is implied that the integral particle extraction rates at $\tau > \tau_{CER}$ do not noticeably depend on the detailed prehistory of the process, $\tau < \tau_{CER} << 1$, when the pore-phase concentration *c* virtually varies with time and along the vessel. The prehistory influence diminishes with time.

The value of S_{CER} depends on *M* and varies from 0.05 to 0.1 at $M \to \infty$ to < 0.01 for the BIC approach at $M \to 0$. The estimates were obtained after analysis of a representative set of data available in the literature [32–35] in terms of the SC submodel and respective asymptotic expansions [12]; the BIC value was predicted by simulations. Therefore, there is an uncertainty in the $\alpha(M)$ determination, depending on the assumed particle-scale regime, since the value $Y(\tau_{CER})$ is fixed in a particular experiment

$$\alpha(M) = \frac{Y(\tau_{CER}) - S_{CER}(M)}{1 - S_{CER}(M)} \tag{18}$$

The assumption of high cell-membrane permeability leads to increased extractability of superficial cells of ordinary particles. This oil fraction contributes to the duration of the initial stage. Hence, the volume fraction α of free-oil receptacles required for supplying the same value $Y(\tau_{CER})$ should be reduced in the limit of large *M* if compared with the deduced value for small *M*.

Asymptotically, the OEC behavior is fully represented by the *S* function, the analysis of which is crucial for understanding how internal diffusional regimes manifest themselves on the macroscale. Numerical solutions of Eqs. (11), (13), and (14) at $c = 0$ are plotted in terms of cumulative function *S* versus normalized time τ in Fig. 3 a at different *M*. Importantly, a linear initial part can be discerned in *S* curves, and its time duration gradually decreases from unity to zero with an increase in *M*; its initial slope $k(M)$ grows accordingly from unity to infinity, and could be approximated as shown in Eq. (19)

$$k(M) = \begin{cases} 1, & \ln M \le -10 \\ 1 + 0.5(0.1\ln M + 1)^{\frac{25}{3}}, & -10 \le \ln M \le 2 \\ \sqrt{M}e^{0.163}, & \ln M > 2 \end{cases} \tag{19}$$

The dependence of *S* on $k\tau$ is shown in Fig. 3 b by solid lines.

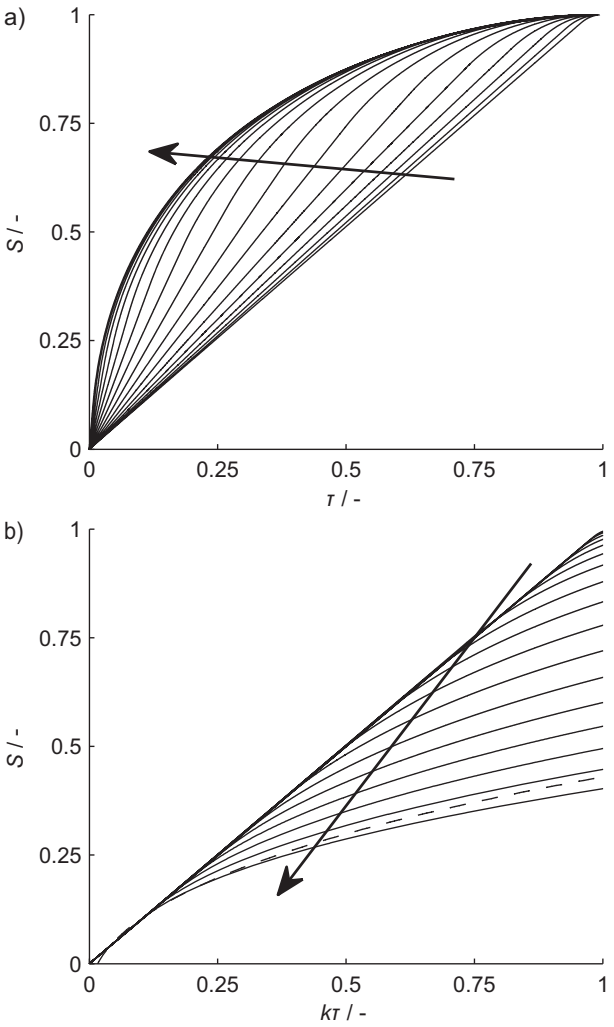

Figure 3. The dependence of cumulative function S on (a) normalized time, and (b) product $k\tau$ at different M values. Arrows indicate ln$M$ increases in steps of 0.5 from −3 to 5.

An initial common linearity and identity of the majority of the integral S curves completely screens any specific features of oil distribution X_s inside particles because timescale T is unknown. As a result, it is impossible to distinguish between different internal regimes within the linear stage, when only a small fraction of tied solute is removed from particles. Overall, not more than 25 % of tied oil is extracted in laboratory experiments [32–35], and S curves remain indistinguishable for $M < 33$ at unknown timescale T.

Yet, in view of the above considerations, it might be thought that different regimes with relatively short linear stages, in which $M > 33$, could be recognized. However, as mentioned above, there is an uncertainty in α, i.e., S_{CER}, determination. In various extraction regimes, different values $\alpha(M)$ should be added to $(1 - \alpha)S$ to obtain the Y function. Equivalently, at large M the S curve can be downshifted by 0.05–0.1, and the initial slope k should be modified to ensure the constant (with respect to M) value of S_{CER}. Such an example is given in Fig. 3 b by a dashed line. The dependence plotted with the dashed curve is $S(\tau) - 0.0723$ at $k = 9$, $M \to \infty$ (SC limit), and closely follows the other curve in the figure. So, regimes at $M > e^5$ (≈ 150) could be confused with the SC limit.

3.3 Particle-Scale Submodel Detection

One-parameter particle-scale submodels are sufficient only for short-time extraction in labs, and they provide the same accuracy in data interpretation. Both limiting approaches analyzed here suggest a first-order approximation of OEC. The same is expected for other simple models. At least two parameters (D_a and β_c) should be identified for extrapolation of experimental data over a large period of time, when predictions of simplified models noticeably deviate from each other.

For illustration, the proposed expansion in Eq. (17) has been used to correlate data available in the literature [32] at different values of D_a and β_c. Three regimes have been simulated at SC and BIC limits as well as in a transitional regime of $M \approx 1$. Deduced values of adaptive parameters together with apparent particle sizes are summarized in Tab. 1, and the corresponding curves are given in Fig. 4 a. All internal regimes closely fit the data on a macroscale level, while the deduced values of D_a and β_c differ noticeably.

Table 1. Particle-scale submodel adaptive parameters for packed beds composed of pumpkin seeds [32] at different assumed extraction regimes[a].

	SC			Intermediate regime			BIC		
Curve number	1	2	3	1	2	3	1	2	3
a [mm]	0.42	0.67	0.96	0.42	0.67	0.96	0.42	0.67	0.96
$D_a \times 10^{11}$ [m^{2}s^{-1}]	0.12	0.12	0.12	1.2	1.2	1.2	1000	1000	1000
$\beta_c \times 10^5$ [s^{-1}]	1000	1000	1000	10	10	10	6.7	6.7	6.7
M [–]	735	1870	3840	0.735	1.87	3.84	4×10^{-4}	1×10^{-3}	2×10^{-3}
α[b] [–]	0.84	0.44	0.29	0.86	0.47	0.31	0.87	0.49	0.32

[a] Conditions: $x_s^0 = 220$ kg m^{-3}, $\theta_* = 7.7$ kg m^{-3}, $P = 30$ MPa, $T = 313$ K, $v = 1.85\times10^{-4}$ m s^{-1}, $H = 5.56$ cm. [b] The variation of α with M is discussed in Sect. 3.2; see Eq. (18).

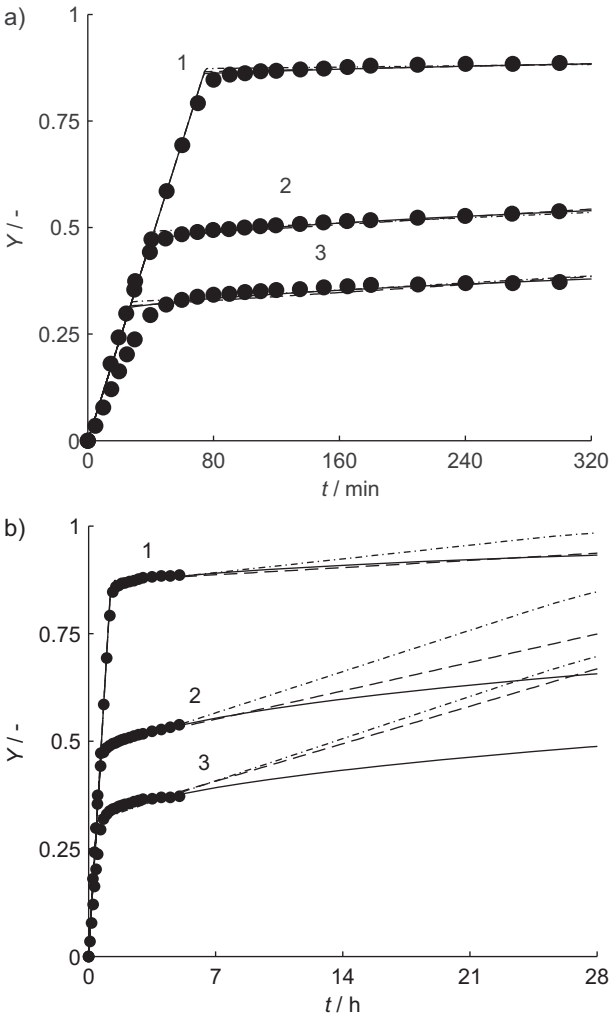

Figure 4. Experimental (dots) [32] and theoretical (lines) OECs. (a) Correlation of experimental data, (b) extrapolation of experimental data using deduced values of diffusional raw-material properties. Solid lines: SC limit; dashed lines: BIC limit; dash-dotted lines: intermediate regime.

The obtained values of adjustable parameters have been used to extend the oil-extraction curves to high times of the process (Fig. 4 b). At a certain moment, OECs corresponding to different microscale regimes, but in identical experimental conditions, start to deviate from each other and a crucial dependence of the total extraction time on the particle-scale submodel is revealed. Importantly, the predicted extraction rates are greater in the case of $M \approx 1$ than in the BIC limit.

The strong sensitivity of OEC to the deduced values of model parameters, i.e., α, D_a, and β_c, and the particle-scale extraction regime suggests a way for detecting a reasonable multiparameter SFE model. A series (2–4 curves) of relatively long (10–20 h) OEC data is needed to specify the extraction regime in the case of a mean particle size in the range 600–1500 μm. Ideally, the corresponding M values should also be in the range of 30–150 to diminish the free-oil receptacle model impact on the data interpretation. The reduction of the free-oil fraction and the packed-bed height should also decrease the uncertainty in the determination of the mass-transport parameters D_a and β_c, as well as in estimation of the full depletion timescale, T.

Another question that could be resolved in the proposed experiment is the relative comparison of the extraction resistances caused by cell membranes (BIC regime) and transport channels (SC regime) for any plant raw material. It can be concluded from the performed computational experiments that higher conductivity or transport channels manifests itself in a continuous decrease of macroscale extraction rates, whereas a constant slope of OEC during a relatively long time interval is indicative of the low cell-membrane permeability.

4 Conclusion

The generalized particle-scale submodel, which explicitly accounts for two types of diffusional resistance in plant raw material has been suggested and studied. The model incorporates the principal assumptions of two well-known literature approaches, SC and BIC, and includes them as limits of high and small M at $\Theta \to 0$, respectively.

The principal limitation of up-to-date experiments is that they only allow identification of the initial extraction rates of tied solute. However, at various internal extraction regimes, these rates either remain constant ($M \to 0$) or decrease ($M \to \infty$) leading to an increase in particle-depletion time. Therefore, the relationship between the typical rates of solute diffusion across the cell membranes and those through the particle, along its transport channels, is an additional model assumption. It is insignificant for experimental data correlation, but it should be validated for confident extrapolation of obtained results to the process over long periods of time.

A set of OECs, corresponding to substrates with different average particle sizes, provides more information for the identification of internal model adaptive parameters at fixed values of pressure and temperature. The lab-scale experiment duration should be increased from 5 to 10–20 hours to detect the limiting mass-transfer mechanism – cell membrane or transport-channels conductivity. Importantly, particle polydispersity, packing inhomogeneity, and the initial linear extraction stage, etc., add to the complexity of model detection with respect to OECs at long process times.

Acknowledgment

This study was supported by the Russian Foundation for Basic Research and by the Academy of Science of Republic of Tatarstan through the grant no. 15-41-02542 r_povolzhe_a and grant no. 16-31-00007 mol_a. This work was funded by the subsidy allocated to Kazan Federal University for the state assignment in the sphere of scientific activities.

The author has declared no conflict of interest.

Symbols used

a	[m]	radius of a spherical particle
c	[kg m^{-3}]	solute concentration in the pore phase
D_a	[m^{2}s^{-1}]	apparent diffusion coefficient in the apoplast
k	[–]	slope of the $S(\tau)$ function at $\tau \to 0$
M	[–]	dimensionless complex, which characterizes ground plant material fraction of size a and defines the internal extraction regime in it, $a^2\beta_c/2D_a$
r	[m]	radial coordinate in the particle with the origin in the particle center
s	[–]	cumulative function for the free oil, volume fraction of oil extracted from free oil receptacle to the current extraction moment, $0 \le s \le 1$
S	[–]	cumulative function for the tied oil, volume fraction of oil extracted from the particle to the current extraction moment, $0 \le S \le 1$
S_{CER}	[–]	value of S at $\tau = \tau_{CER}$
t	[s]	time
T	[s]	characteristic time of particle depletion
x_s	[kg m^{-3}]	average density of oil currently contained in the cell, including the one dissolved in the solvent and undissolved oil
x_s^0	[kg m^{-3}]	initial average density of oil contained in the cell
X_s	[–]	normalized average density of oil currently contained in the cell, x_s/x_s^0
Y	[–]	overall extraction curve, $0 \le Y \le 1$

Greek letters

α	[–]	volume fraction of raw material that contains free solute
β_c	[s^{-1}]	reduced cell membrane permeability coefficient
δ_a	[–]	dimensionless number that characterizes the solute accumulation capacity of the apoplast, $\varepsilon_a\theta_*/x_s^0$
Δ	[m^{-2}]	Laplace operator
ε_a	[–]	particle volume fraction, occupied by the apoplast
ε_{is}	[–]	cell volume fraction, occupied by insoluble substances
ζ	[–]	normalized axial coordinate in the vessel varying along the flow, $0 \le \zeta \le 1$
θ_a	[kg m^{-3}]	solute concentration in the apoplast
θ_s	[kg m^{-3}]	solute concentration in the symplast
θ_*	[kg m^{-3}]	solute saturation concentration in both phases (solid and liquid)
ϑ_a	[–]	normalized solute concentration in the apoplast, θ_a/θ_*
ϑ_s	[–]	normalized solute concentration in the symplast, θ_s/θ_*
Θ	[–]	dimensionless complex that characterizes solvent dissolution capacity, $(1 - \varepsilon_{is})\theta_*/x_s^0$
ξ	[–]	normalized radial coordinate in the particle, $r = \xi$ a
τ	[–]	normalized time, t/T
τ_{CER}	[–]	end of linear extraction stage of SFE process

Subscripts

a	apoplast
BIC	limit of the BIC approach
s	symplast
SC	limit of the SC approach

Abbreviations

BIC	broken and intact cells
CER	constant extraction rate
MRI	magnetic resonance imaging
OEC	overall extraction curve
SC	shrinking core
SFE	supercritical fluid extraction

References

[1] *Green Chemistry: Theory and Practice* (Eds: P. T. Anastas, J. C. Warner), Oxford University Press, Oxford **1998**.

[2] G. Brunner, *Annu. Rev. Chem. Biomol. Eng.* **2010**, *1*, 321–342. DOI: 10.1146/annurev-chembioeng-073009-101311

[3] E. Schutz, *Chem. Eng. Technol.* **2007**, *30 (6)*, 685–688. DOI: 10.1002/ceat.200600297

[4] J. M. del Valle, *J. Supercrit. Fluids* **2015**, *96*, 180–199. DOI: 10.1016/j.supflu.2014.10.001

[5] M. Bravi, R. Bubbico, F. Manna, N. Verdone, *Chem. Eng. Sci.* **2002**, *57 (14)*, 2753–2764. DOI: 10.1016/S0009-2509(02)00145-8

[6] L. Fiori, *Chem. Eng. Process* **2010**, *49 (8)*, 866–872. DOI: 10.1016/j.cep.2010.06.001

[7] A. A. Salamatin, A. G. Egorov, *J. Supercrit. Fluids* **2015**, *105*, 35–43. DOI: 10.1016/j.supflu.2015.01.013

[8] A. G. Egorov, A. A. Salamatin, *Russ. Math.* **2015**, *59 (2)*, 48–56. DOI: 10.3103/S1066369X15020073

[9] L. Fiori, D. Calcagno, P. Costa, *J. Supercrit. Fluids* **2007**, *41 (1)*, 31–42. DOI: 10.1016/j.supflu.2006.09.005

[10] X. Han, L. Cheng, R. Zhang, J. Bi, *J. Food Eng.* **2009**, *92*, 370–376. DOI: 10.1016/j.jfoodeng.2008.12.002

[11] M. Goto, B. C. Roy, T. Hirose, *J. Supercrit. Fluids* **1996**, *9 (2)*, 128–133. DOI: 10.1016/S0896-8446(96)90009-1

[12] A. G. Egorov, A. A. Salamatin, *Chem. Eng. Technol.* **2015**, *38 (7)*, 1203–1211. DOI: 10.1002/ceat.201400627

[13] H. Sovova, *Chem. Eng. Sci.* **1994**, *49 (3)*, 409–414. DOI: 10.1016/0009-2509(94)87012-8

[14] H. Sovova, *J. Supercrit. Fluids* **2012**, *66*, 73–79. DOI: 10.1016/j.supflu.2011.11.004

[15] L. Fiori, D. Basso, P. Costa, *J. Supercrit. Fluids* **2009**, *48 (2)*, 131–138. DOI: 10.1016/j.supflu.2008.09.019

[16] C. Marrone, M. Poletto, E. Reverchon, A. Stassi, *Chem. Eng. Sci.* **1998**, *53 (21)*, 3711–3718. DOI: 10.1016/S0009-2509(98)00150-X

[17] E. L. G. Oliveira, A. J. D. Silvestre, C. M. Silva, *Chem. Eng. Res. Des.* **2011**, *89 (7)*, 1104–1117. DOI: 10.1016/j.cherd.2010.10.025
[18] Z. Zekovic, S. Filip, S. Vidovic, S. Jokic, S. Svilovic, *Chem. Eng. Technol.* **2014**, *37 (12)*, 2123–2128. DOI: 10.1002/ceat.201400322
[19] A. Rai, K. D. Punase, B. Mohanty, R. Bhargava, *Int. J. Heat Mass Transfer* **2014**, *72*, 274–287. DOI: 10.1016/j.ijheatmasstransfer.2014.01.011
[20] V. Abrahamsson, N. Andersson, B. Nilsson, C. Turner, *J. Supercrit. Fluids* **2016**, *111*, 14–27. DOI: 10.1016/j.supflu.2016.01.006
[21] M. Poletto, E. Reverchon, *Ind. Eng. Chem. Res.* **1996**, *35 (10)*, 3680–3686. DOI: 10.1021/ie9600093
[22] A. K. K. Lee, N. R. Bulley, M. Fattori, A. Meisen, *J. Am. Oil Chem. Soc.* **1986**, *63 (7)*, 921–925. DOI: 10.1007/BF02540928
[23] J. M. del Valle, P. Napolitano, N. Fuentes, *Ind. Eng. Chem. Res.* **2000**, *39*, 4720–4728. DOI: 10.1021/ie000034f
[24] E. F. Moura, M. C. Ventrella, S. Y. Motoike, *Sci. Agric.* **2010**, *67 (4)*, 399–407. DOI: 10.1590/S0103-90162010000400004
[25] D. M. Joel, H. Bar, A. M. Mayer, D. Plakhine, H. Ziadne, J. H. Westwood, G. E. Welbaum, *Ann. Bot.* **2012**, *109 (1)*, 181–195. DOI: 10.1093/aob/mcr261
[26] A. Femenia, M. Garcia-Marin, S. Simal, C. Rossello, M. Blasco, *J. Agric. Food Chem.* **2001**, *49 (12)*, 5828–5834. DOI: 10.1021/jf010532e
[27] A. Lehner, F. Corbineau, C. Bailly, *Plant Cell Physiol.* **2006**, *47 (7)*, 818–828. DOI: 10.1093/pcp/pcj053
[28] B. Honarvar, S. A. Sajadian, M. Khorram, A. Samimi, *Braz. J. Chem. Eng.* **2013**, *30 (1)*, 159–166. DOI: 10.1590/S0104-66322013000100018
[29] Y. Liu, Y. Zhao, J. Zhao, Y. Song, *Magn. Reson. Imaging* **2010**, *29 (8)*, 1110–1118. DOI: 10.1016/j.mri.2011.05.009
[30] A. G. Egorov, A. A. Salamatin, R. N. Maksudov, *Theor. Found. Chem. Eng.* **2014**, *48 (1)*, 39–47. DOI: 10.1134/S0040579514010011
[31] A. A. Salamatin, *IOP Conf. Ser.: Mater. Sci. Eng.* **2016**, *158*, 012081. DOI: 10.1088/1757-899X/158/1/012081
[32] U. Salgin, H. Korkmaz, *J. Supercrit. Fluids* **2011**, *58 (2)*, 239–248. DOI: 10.1016/j.supflu.2011.06.002
[33] S. G. Ozkal, M. E. Yener, L. Bayindirli, *J. Supercrit. Fluids* **2005**, *35 (2)*, 119–127. DOI: 10.1016/j.supflu.2004.12.011
[34] L. Fiori, *J. Supercrit. Fluids* **2009**, *50 (3)*, 218–224. DOI: 10.1016/j.supflu.2009.06.011
[35] L. Fiori, *J. Supercrit. Fluids* **2007**, *43 (1)*, 43–54. DOI: 10.1016/j.supflu.2007.04.009

